Article

Study of Magnetic Properties and Relaxation Time of Nanoparticle Fe$_3$O$_4$-SiO$_2$

Togar Saragi * , **Bayu Permana, Arnold Therigan, Hotmas D. Sinaga, Trisna Maulana and Risdiana Risdiana**

Department of Physics, Faculty of Mathematics and Natural Sciences, Universitas Padjadjaran, Jl. Raya Bandung-Sumedang km 21, Jatinangor, Sumedang 45363, Indonesia; bayubaper@gmail.com (B.P.); arnoldtherigan15@gmail.com (A.T.); hotmas28@gmail.com (H.D.S.); trisna17002@mail.unpad.ac.id (T.M.); risdiana@phys.unpad.ac.id (R.R.)
* Correspondence: t.saragi@phys.unpad.ac.id

Abstract: The magnetic properties and relaxation time of Fe$_3$O$_4$ nanoparticles, and their encapsulation with silicon dioxide (Fe$_3$O$_4$-SiO$_2$), have been successfully investigated by analyzing the temperature dependence of magnetization ($M(T)$) and the time dependence of magnetization ($M(t)$), using the SQUID magnetometer measurement. The $M(T)$ measurement results can determine the magnetic parameters and magnetic irreversibility of Fe$_3$O$_4$ and Fe$_3$O$_4$-SiO$_2$ samples. The values of Curie constant (C), effective magnetic moment (μ_{eff}), and Weiss temperature (θ_P) are 4.2 (emu.K.Oe/mol), 5.77 μ_B, and -349 K, respectively, for the Fe$_3$O$_4$ samples, and 81.3 (emu.K.Oe/mol), 25.49 μ_B, and -2440 K, respectively, for the Fe$_3$O$_4$-SiO$_2$ samples. After encapsulation, the broadening peak deviation decreased from 281.6 K to 279 K, indicating that the superparamagnetic interactions increased with the encapsulation process. The magnetic parameters and irreversibility values showed that the superparamagnetic properties increased significantly after encapsulation (Fe$_3$O$_4$-SiO$_2$). From the results of the $M(t)$ measurement, it was found that there was a decrease in the magnetic relaxation time after the encapsulation process, which indicated that the distribution of the nanoparticle size and anisotropy energy increased.

Keywords: encapsulation; Fe$_3$O$_4$ nanoparticle; irreversibility; relaxation time; SiO$_2$; superparamagnetic

1. Introduction

Fe-based materials are magnetic materials that have many functions and applications that can be developed. The most studied Fe-based materials are Fe$_2$O$_3$ and Fe$_3$O$_4$. These two materials have different characteristics that can be utilized for specific applications. In the bulk state, the Fe$_2$O$_3$ material has antiferromagnetic and weak ferromagnetism properties in a certain temperature range, while the Fe$_3$O$_4$ material has ferrimagnetic properties in the entire temperature range [1]. Fe$_3$O$_4$ is a material that has widely attracted attention to be studied, especially for several applications, such as in ferrofluids [2], magnetic refrigeration, the detoxification of biological fluids, and the magnetically controlled transport of anticancer drugs [3,4]. This material is still open and exciting to study, especially at the nano size. At the nanoparticle size, Fe$_3$O$_4$ has superparamagnetic properties, where the magnetization can fluctuate thermally. The magnetic saturation is high, and the coercivity and remanence are equal to zero. Therefore, this nanoparticle can be delivered to the tissue target without agglomeration, and can easily be controlled by a magnetic field [5]. Fe$_3$O$_4$ is quite a stable compound compared to Fe$_2$O$_3$, so it is very suitable for observing various magnetic properties of the material.

The superparamagnetic state can be realized through encapsulation processes, such as SiO$_2$ [3,4] and oleic acid [6]. This process aims to prevent agglomeration, maintain the magnetic stability of the material, and reduce the cytotoxic effect. In this study, SiO$_2$ was chosen as a ligand to modify the surface of the Fe$_3$O$_4$ nanoparticles. SiO$_2$ is a compound that has good chemical stability, good hydrophilicity, and has a surface hydroxyl group

that allows further modification. In addition, SiO_2 is not easy to agglomerate during the synthesis process, undergoes intermolecular redox reactions, and can reduce the cytotoxic effect of the Fe_3O_4 nanoparticles when applied for various biomedical purposes [4].

The magnetic properties of nanoparticles, both Fe_3O_4 and Fe_3O_4-SiO_2, are very important to study. These magnetic characteristics can provide information about important parameters that can be considered in their development and utilization for various applications. One of these characteristics is the temperature dependence of magnetization $M(T)$ and the time dependence of magnetization $M(t)$. The information obtained from the $M(T)$ measurement includes the type of magnetic material, the blocking temperature, the critical temperature, and the effective magnetic moment [1,7–9], while the $M(t)$ measurement obtained relaxation time information. The relaxation time is a measure of the rotational freedom of magnetic nanoparticles, which provides information on several material characteristics, such as the viscosity, chemical bonding, and stiffness of the matrix to which the nanoparticles are bonded. This characteristic is an important parameter for biological applications [10].

In previous research, we have analyzed $M(T)$ data on the ZFC process for Fe_3O_4 and Fe_3O_4-SiO_2 nanoparticles, to obtain information on the effect of SiO_2 encapsulation on the blocking temperature of the Fe_3O_4 material. We found that the blocking temperature increased after the encapsulation process [8]. The value of T_C has also been reported for Fe_3O_4-SiO_2, by measuring the samples in the temperature range of 300–900 K and a magnetic field of 10 kOe. It was found that T_C is ~850 K [11]. Therefore, the value of T_C and other magnetic properties in the temperature range of 10–300 K still need to be determined. In addition, the effect of SiO_2 encapsulation to Fe_3O_4 on the effective magnetic moment and relaxation time has not been widely reported. This information is beneficial for its development and application in biomedicine, which is difficult to obtain from in vivo research.

Here, we reported the magnetic properties of the Fe_3O_4 and Fe_3O_4-SiO_2 nanoparticles, namely, the Curie constant (C), effective magnetic moment (μ_{eff}), Weiss temperature (θ_P) from the $M(T)$ measurement in the FC process, and the relaxation time (τ) from the $M(t)$ measurement [12]. We also analyzed the magnetothermal properties by plotting $[-d(M_{FC} - M_{ZFC})/dT]$ versus temperature. This analyst will provide information regarding peak broadening, which describes the distribution of nanoparticles, concerning the anisotropic energy of the system [13–15].

2. Materials and Methods

Magnetic nanoparticles of Fe_3O_4 were synthesized by the co-precipitation method. The precursors of Fe^{2+} and Fe^{3+} cations are ferric chlorid hexahydrate, $FeCl_3·6H_2O$ (CAS No. 10025-77-1, Sigma-Aldrich, St. Louis, MI, USA), and iron (II) chloride tetrahydrate puriss. p.a, $FeCl_2·4H_2O$ (CAS No. 13478-10-9, Sigma-Aldrich, St. Louis, MI, USA), respectively. A total of 5.41 g of $FeCl_3·6H_2O$ and 1.99 g of $FeCl_2·4H_2O$ were dissolved in 100 mL of DI water, then stirred for 30 min at 25 °C. Experiment details are described in our previous publications [16].

2.1. Synthesis of Fe_3O_4 Nanoparticles

From 100 mL of the solution resulting from mixing $FeCl_3·6H_2O$ and $FeCl_2·4H_2O$ precursors, 25 mL of the solution was separated, and 25% NH_4OH was added dropwise until pH = 10. Then the solution was stirred and sonicated for 30 min. In this study, the sonication process was carried out simply by using a sonication bath (Branson M1800-E, CPX-952-136R, Shanghai, China) without a sonicator tip. The sonication bath was filled with water, and a beaker glass containing the magnetite solution was placed into the sonication bath. The frequency used in the sonication bath was 40 kHz. This ultrasonic wave was delivered to a glass beaker containing a magnetite solution through water in the sonication bath. After sonication, the solution was allowed to stand for 30 min to obtain a

precipitate of magnetite nanoparticles. The precipitate formed was washed with n-hexane and re-dispersed into DI water. The sample obtained is referred to as Fe_3O_4.

2.2. Synthesis of Fe_3O_4-SiO_2 Nanoparticles

From 75 mL of the remaining solution resulting from mixing $FeCl_3 \cdot 6H_2O$ and $FeCl_2 \cdot 4H_2O$ precursors, 25 mL of the solution was separated again, and 0.4 mL of tetraethyl orthosilicate (TEOS) was added, and, finally, 25% NH_4OH was added dropwise until pH = 10. The same process was carried out as the synthesis process of Fe_3O_4. The sample is referred to as Fe_3O_4-SiO_2.

2.3. Characterization

All samples were characterized by using high-resolution transmission electron microscopy (HR-TEM H9500, Hitachi High-Tech, Tokyo, Japan) to measure the particle size. The temperature dependence of magnetization $M(T)$ in zero fields cooled (*ZFC*) and field cooled (*FC*), with the external magnetic field of 100 Oe at 10–300 K, was measured by a superconducting quantum interference device (SQUID) Magnetometer (Quantum Design MPMS XL, San Diego, CA, USA). We also measured the time dependence of magnetization $M(t)$ to investigate the relaxation time of magnetite Fe_3O_4 and Fe_3O_4-SiO_2. The SQUID measurements were carried out in the Graduate School of Engineering, Tohoku University, Japan.

3. Results and Discussion

3.1. Particle Size of Fe_3O_4 and Fe_3O_4-SiO_2 Nanoparticles

Figure 1 shows HR-TEM images of the Fe_3O_4 (a) and Fe_3O_4-SiO_2 (b) samples. In general, the morphology of the two samples was nearly spherical. The Fe_3O_4 sample shows a clear boundary, while the Fe_3O_4-SiO_2 sample shows a shadow boundary, which is believed to be the result of the encapsulation process. It can also be observed that the particle size of the Fe_3O_4 sample is 11 ± 2.22 nm, while the particle size of the core Fe_3O_4-SiO_2 sample is 10 ± 1.53 nm.
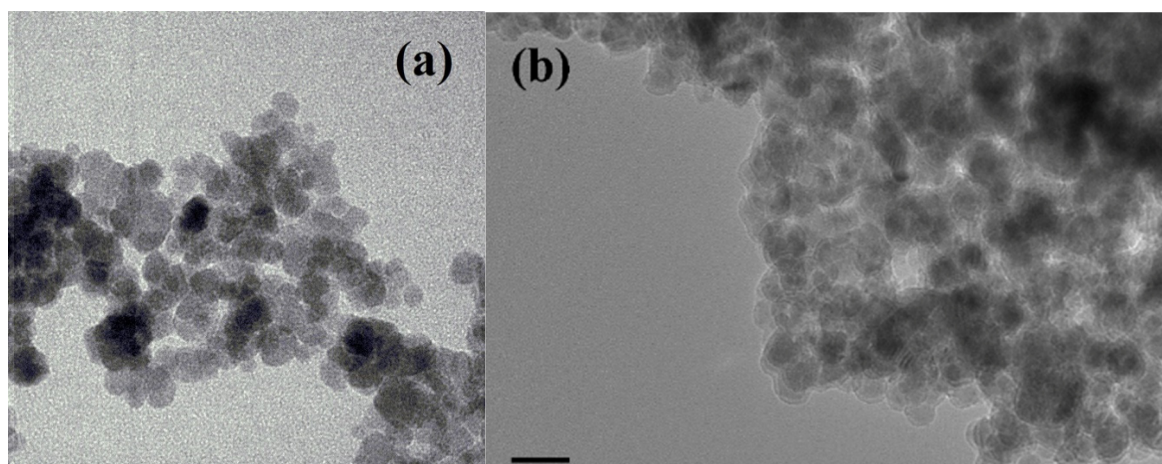

Figure 1. HR-TEM images of sample Fe_3O_4 (**a**) and Fe_3O_4-SiO_2 (**b**).

3.2. Temperature Dependence of Magnetization, $M(T)$

The results of the temperature dependence of the magnetization of $M(T)_{FC}$ and $M(T)_{ZFC}$ for the Fe_3O_4 (a) and Fe_3O_4-SiO_2 (b) nanoparticles are shown in Figure 2.

From Figure 2a, it can be observed that the magnetization value of Fe_3O_4 slowly increases when the temperature is lowered to about 100 K, for both *ZFC* and *FC*. At temperatures below 100 K in the *ZFC* process, the magnetization value decreases sharply, while, in the *FC* process, the magnetization value tends to be independent of temperature below about 80 K. From Figure 1b, it can be observed that changes in the magnetization

value of Fe_3O_4-SiO_2 occur at a higher temperature range. The value of magnetization in the *ZFC* process, after encapsulation, increased when the temperature decreased from 300 K to 217 K, and then decreased when the temperature decreased to 10 K. In the *FC* process, the magnetization value tends to increase slightly as the temperature decreases from 300 K to 10 K.
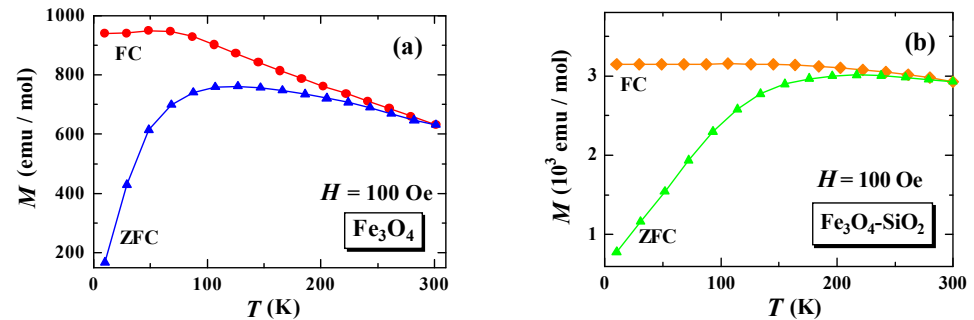

Figure 2. Temperature dependence of magnetization of Fe_3O_4 (**a**) and Fe_3O_4-SiO_2 (**b**) nanoparticles.

Figure 2 also shows the characteristics of magnetic irreversibility, which reveals differences in the magnetization values of M_{FC} and M_{ZFC} in the entire measurement temperature range. It indicates a thermally induced magnetic relaxation process. The effect of magnetic irreversibility is shown in Fe_3O_4 and Fe_3O_4-SiO_2, where the M_{FC} and M_{ZFC} branches meet at 300 K. Although these branches do not overlap below 300 K, it can be observed that Fe_3O_4 and Fe_3O_4-SiO_2 exhibit superparamagnetic characteristics. The branching point temperature of the M_{FC} and M_{ZFC} in the Fe_3O_4-SiO_2 sample is lower than that in the Fe_3O_4 sample, namely, at temperatures around 261 K and 300 K, respectively. This is in accordance with the H_C coercivity value for the Fe_3O_4-SiO_2 sample, which is lower than that of the Fe_3O_4 samples, which are 25.99 Oe and 362.37 Oe, respectively [16].

3.3. Curie Temperature (T_C)

This change in the magnetization tendency to temperature can be further analyzed to determine the Curie temperature. Figure 3 shows the magnetization derivative curve of $M(T)_{FC}$ to the temperature (dM/dT) of Fe_3O_4. From the curve (dM/dT) versus T at the minimum peak, we can estimate the Curie temperature (T_C) of the sample [9,11]. From Figure 3, it can be estimated that the T_C value for Fe_3O_4 is 125 K. This value is relatively smaller than that reported by Blundell, which is 858 K [17], probably due to differences in particle size or cation vacancies. As reported in previous studies, the T_C value increases with decreasing particle size [18] or increasing cation vacancies [11]. On the other hand, the Curie temperature of the encapsulated Fe_3O_4 with SiO_2 could not be determined. This is because there is no significant change in magnetization (M_{FC}) when the temperature is lowered, as shown in Figure 2b, so the minimum peak of the first derivative (dM/dT) is not obtained.

3.4. Curie Constant, Effective Magnetic Moment, and Weiss Temperature

The values of C, μ_{eff}, and θ_P can be determined by using the Curie–Weiss law in Equations (1) and (2). The value of the Curie constant is obtained through the following regression equation (Equation (1)) of the inverse molar susceptibility curve (χ^{-1}) versus temperature (T):

$$\chi_m = \frac{C}{(T - \theta_P)} \tag{1}$$

$$C = \frac{N_A}{3k_B}\mu_{eff}^2\mu_B^2 \tag{2}$$

where C is the Curie constant, defined as Equation (2), θ_P is the Weiss temperature, N_A is Avogadro's number, k_B is the Boltzmann constant, and μ_B is the Bohr mag-

neton. From Equation (2), the value of the effective magnetic moment is obtained ($\mu_{eff} = \sqrt{3Ck_B/N_A\mu_B^2} = 2.828\sqrt{C}$) [9,19]. From Equation (1), the Curie constant and the Weiss temperature can be obtained through the regression equation (χ^{-1}) versus temperature (T), as shown in Figure 4.
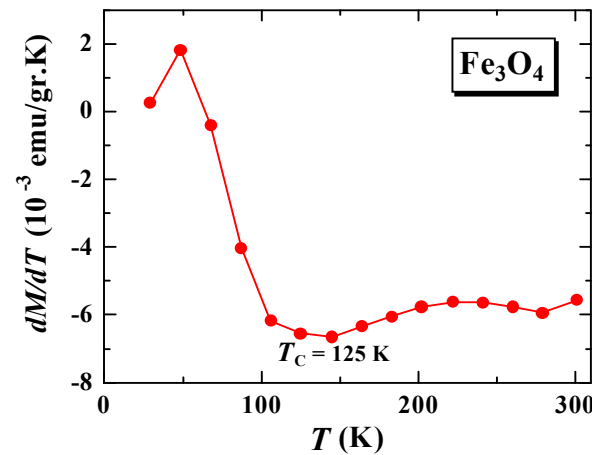

Figure 3. The first derivative curve of $M(T)_{FC}$ versus temperature of sample Fe_3O_4.
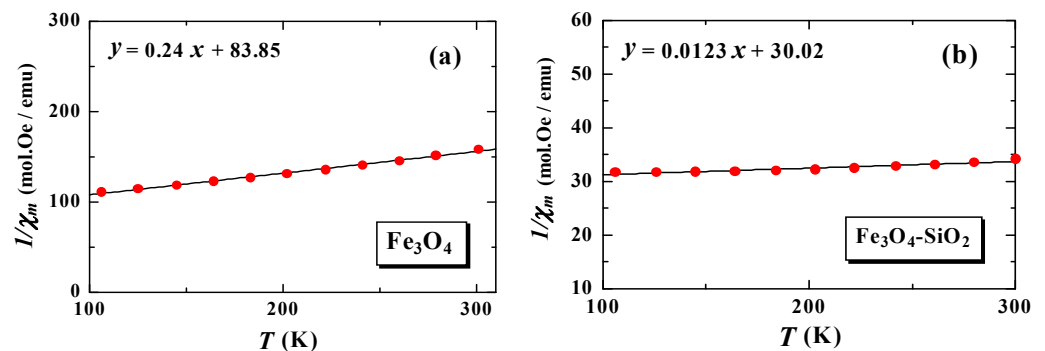

Figure 4. The fitting of Curie–Weiss law on M_{FC} data of Fe_3O_4 (**a**) and Fe_3O_4-SiO_2 (**b**).

By using the C value from the fitting and Equation (2), the effective magnetic moment value is obtained. These magnetic quantities are shown in Table 1. For reference, we also displayed the H_C values for the Fe_3O_4 and Fe_3O_4-SiO_2 samples [16].

Table 1. The magnetic quantities of Fe_3O_4 and Fe_3O_4-SiO_2.

Sample	C (emu.K.Oe/mol)	μ_{eff} (μ_B/fu)	θ_P (K)	H_C (Oe) [16]
Fe_3O_4	4.2 ± 0.01	5.77 ± 0.11	-349 ± 1.03	362.37
Fe_3O_4-SiO_2	81.3 ± 4.20	25.49 ± 2.05	-2440 ± 126.05	25.99

From Table 1, it can be observed that the effective magnetic moment of Fe^{3+} in the Fe_3O_4 sample is 5.77 μ_B. This value is very compatible with the experimental and theoretical results reported by Zatsiupa et al., for the case of $Bi_{25}FeO_{39}$ at a temperature of 5–950 K and a magnetic field of 0.86 T [19]. From these experimental and theoretical results, the values of the effective magnetic moments of the Fe^{3+} ion are reported as 5.82 μ_B and 5.92 μ_B, respectively [19]. The value of the effective magnetic moment of the sample after encapsulation (Fe_3O_4-SiO_2) increased four times, from 5.77 μ_B to 25.49 μ_B. This increment is probably due to the emergence of superparamagnetism from single-domain nanomagnets. In one unit cell of the FCC Fe_3O_4 or $(Fe^{2+})[Fe_2^{3+}]O_4$ system, there are eight bivalent Fe^{2+} cations in the tetrahedral site, which are antiparallel to four cations. Another trivalent is Fe^{3+}, so the effective moment of Fe_3O_4-SiO_2 is four times higher than that of Fe_3O_4

before encapsulation [17]. The effective magnetic moment of a nanoparticle increases with a decrease in the particle size. Increasing the value of μ_{eff} by four times is expected to reduce the value of the magnetic force by up to four times [1], to eliminate the suspected target, if Fe_3O_4-SiO_2 was applied as the material for magnetic hyperthermia applications.

3.5. Distribution of the Anisotropy Energy Barriers

The distribution of the anisotropic energy barriers of the system, which is closely related to the distribution of nanoparticle size and blocking temperature [13–15], can be analyzed through the M_{FC} and M_{ZFC} derivative curves to temperature, $[-d(M_{FC} - M_{ZFC})/dT]$. Figure 5 shows the derivative curve of $[-d(M_{FC} - M_{ZFC})/dT]$ versus the temperature of the Fe_3O_4 and Fe_3O_4-SiO_2 samples.
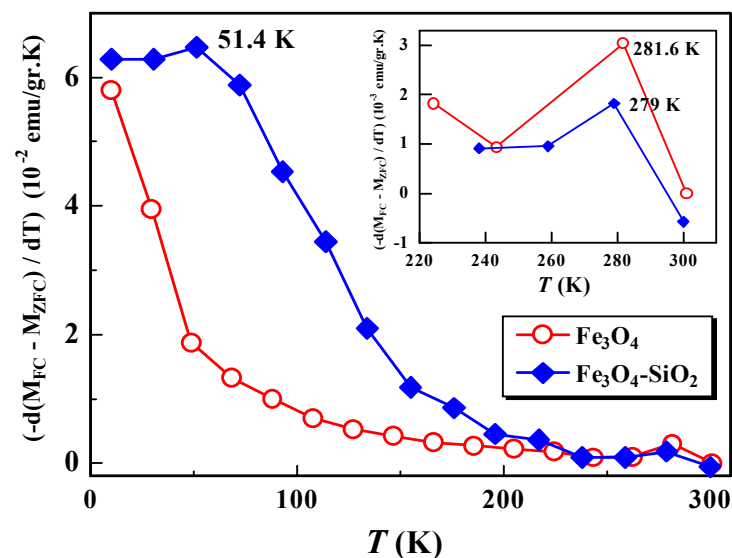

Figure 5. Temperature derivative $[-d(M_{FC} - M_{ZFC})/dT]$ of the difference between *FC* and *ZFC* magnetizations for samples Fe_3O_4 and Fe_3O_4-SiO_2.

From Figure 5, it can be observed that the Fe_3O_4 sample has one broadening peak at a temperature of 281 K, while the Fe_3O_4-SiO_2 sample has a broadening peak at two temperatures, namely, 51.4 K and 279 K. At high temperatures, the broadening peak after encapsulation shifts to lower temperatures, from 281.6 K to 279 K. This indicates that there is dependence of the energy distribution of the barrier on the encapsulation process, which is also related to the nanoparticle size distribution [14]. On the other hand, the shift also indicates relaxation of the almost free assembly of particles, due to superparamagnetism interactions. At low temperatures, the broadening peak of the Fe_3O_4 samples was not observed, probably due to the limitation of the measurement range. We hypothesize that the peak temperature broadening of the Fe_3O_4 sample in the temperature range below 51.4 K might be observed if we conducted the measurement in a narrower temperature range. From our previous study, it has been reported that the blocking temperature and anisotropy energy (ΔE) of Fe_3O_4 and its encapsulated Fe_3O_4-SiO_2 are 118.38 K and 209.03 K, and $3.0 \times 10^3\ k_B$ and $5.2 \times 10^3\ k_B$, respectively [8]. An increase in the blocking temperature value, caused by the encapsulation process, indicates an increase in magnetic interactions between the nanoparticles, resulting in an increase in anisotropic energy barriers, causing the reversal of the magnetization. This is similar to the results obtained by Del Bianco et al., for the case of Fe_3O_4, with various applied fields [14].

3.6. Magnetic Relaxation Time, $M(t)$

Figure 6 shows the magnetization versus time curve after the external magnetic field is quenched to zero, and following curve fitting. Figure 6a,c, show the magnetization versus

time curve for Fe_3O_4 at 10 K and 300 K, while Figure 6e shows the magnetization versus time curve for Fe_3O_4-SiO_2 at 10 K. Figure 6b,d show the curve fittings, using Equation (3), for Fe_3O_4 at 10 K and 300 K, while Figure 6f shows the fitting curve, using Equation (3), for a sample of Fe_3O_4-SiO_2 at 10 K. The measurement results show that the magnetic particles relax when the external magnetic field is quenched. The characteristics of relaxation time can be analyzed using Equation (3), as follows:
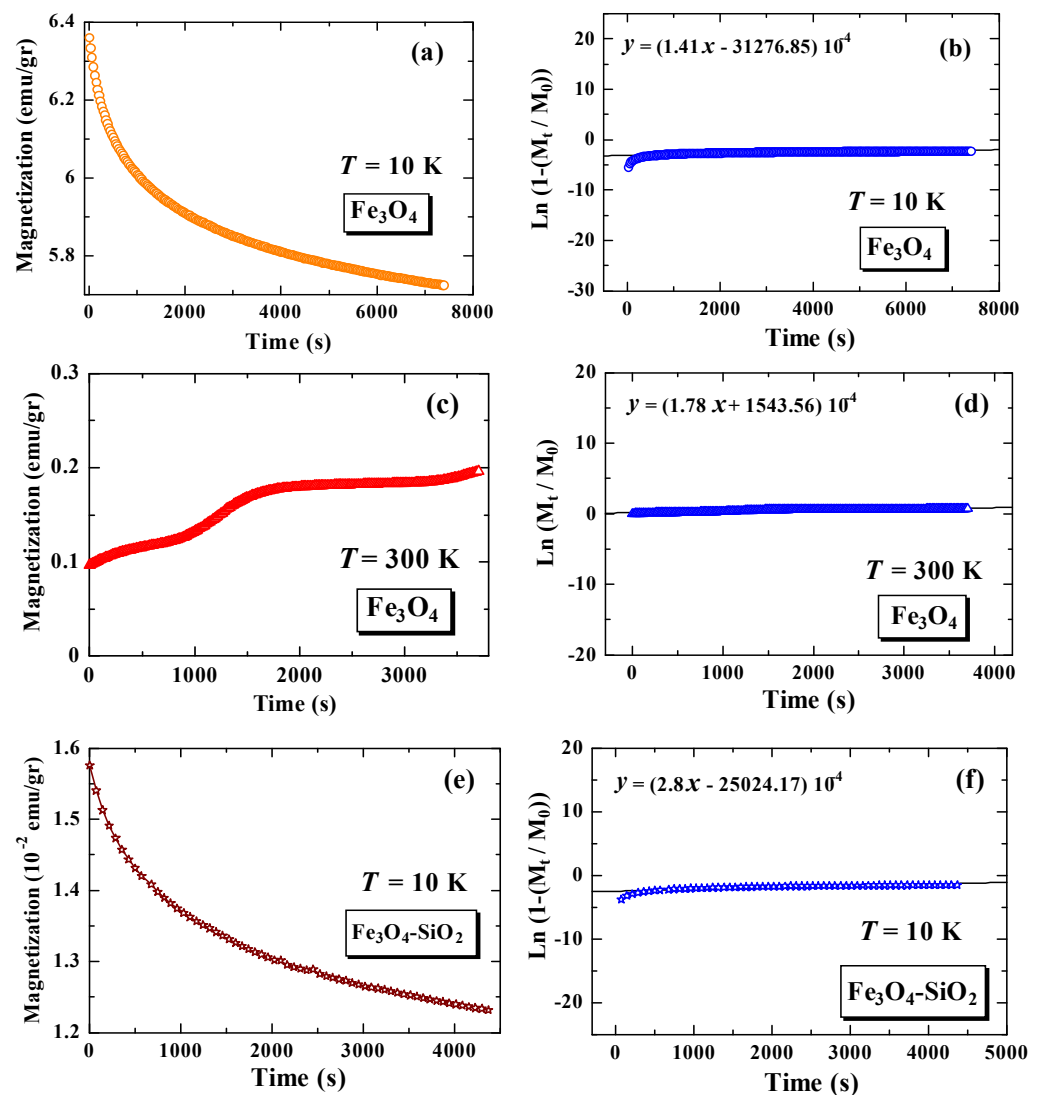
$$M(t) = M(0) \exp\left(\frac{t}{\tau}\right) \tag{3}$$

Figure 6. Time dependence of magnetization for Fe_3O_4 at T = 10 K (**a**), fitting curve of Fe_3O_4 at T = 10 K (**b**), Fe_3O_4 at T = 300 K (**c**), fitting curve of Fe_3O_4 at T = 300 K (**d**), Fe_3O_4-SiO_2 at T = 10 K (**e**), and fitting curve of Fe_3O_4-SiO_2 at T = 10 K (**f**).

The results of the calculation of the relaxation time value for each measurement are arranged in Table 2. The magnetic relaxation times of Fe_3O_4 at 10 K and 300 K are 7.10×10^3 s and 5.62×10^3 s, respectively, while the relaxation time of Fe_3O_4-SiO_2, after encapsulation, decreased to 3.57×10^3 s. In general, the relaxation time of the Fe_3O_4 nanoparticles is greater than that of the Fe_3O_4-SiO_2 nanoparticles after encapsulation. The lower relaxation times are associated with better superparamagnetic properties. These better superparamagnetic properties are supported by the H_C value of the Fe_3O_4-SiO_2

sample (H_C = 25.99 Oe), which is much lower than the H_C value of the Fe_3O_4 sample (H_C = 362.37 Oe) [16]. The lower relaxation time is also associated with an increase in the concentration of nanoparticles in Fe_3O_4-SiO_2 [7]. The decrease in relaxation time in Fe_3O_4, after being encapsulated with SiO_2, can also be related to changes in the anisotropic energy value of the nanoparticles, where the anisotropic energy is also related to the blocking temperature [8,14,20,21]. In our previous study, it was reported that the anisotropic energy of the nanoparticles increased when the Fe_3O_4 samples were encapsulated with SiO_2. The anisotropic energy of the Fe_3O_4 nanoparticles is 3.00×10^3 k_B, while for the Fe_3O_4-SiO_2 nanoparticles, it is 5.20×10^3 k_B [8]. It is clarified that the value of relaxation time decreases when the value of anisotropic energy is increased. The decrease in relaxation time after encapsulation can be correlated with the decrease in medium viscosity, which becomes potential information for biomedical applications [22].

Table 2. The magnetic relaxation time of Fe_3O_4 and Fe_3O_4-SiO_2 nanoparticles.

Sample	T (K)	$\tau \times 10^3$ (s)
Fe_3O_4	10	7.10 ± 1.83
Fe_3O_4	300	5.62 ± 0.49
Fe_3O_4-SiO_2	10	3.57 ± 0.67

In order to obtain more comprehensive information, it is necessary to conduct further research on the magnetic properties and relaxation time, depending on the size of the core Fe_3O_4. In addition, it is also necessary to study the relaxation time depending on the magnetic field. This study is very important to provide information about material properties for biomedical applications that cannot be obtained from in vivo studies.

4. Conclusions

The magnetic properties of Fe_3O_4 and its encapsulation with SiO_2 (Fe_3O_4-SiO_2) have been successfully investigated by analyzing the $M(T)$ and $M(t)$ curves of the SQUID magnetometer measurements. The $M(T)$ curve for the Fe_3O_4 and Fe_3O_4-SiO_2 materials show superparamagnetic properties with magnetic irreversibility characteristics. After encapsulation, the broadening peak of the first derivative of the difference between field-cooled and zero-field-cooled magnetization shifted from 281.6 K to 279 K, which indicates that the Fe_3O_4-SiO_2 material has better superparamagnetic properties than the Fe_3O_4 sample. The values of C, μ_{eff}, and θ_P increased significantly after encapsulation, which also supported the enhancement of the superparamagnetic properties of Fe_3O_4-SiO_2. The value of the effective magnetic moment after encapsulation increased four times, from 5.77 μ_B to 25.49 μ_B. This increment is probably due to the emergence of superparamagnetism from single-domain nanomagnets. Increasing the value of μ_{eff} by four times is expected to reduce the value of the magnetic force to eliminate the suspected target in magnetic hyperthermia applications.

The $M(t)$ curve for Fe_3O_4 and Fe_3O_4-SiO_2 shows that the magnetic relaxation time of the Fe_3O_4-SiO_2 sample decreases compared to the magnetic relaxation time of Fe_3O_4. The lower relaxation times are associated with better superparamagnetic properties. This also indicates that the superparamagnetic properties increase with the encapsulation process. The decrease in relaxation time after encapsulation, from 7.10×10^3 s to 3.57×10^3 s, can be correlated with the decrease in medium viscosity, which becomes potential information for biomedical applications.

In order to obtain more comprehensive information, it is necessary to conduct further research on the magnetic properties and relaxation time, depending on the size of the core Fe_3O_4, to provide information about material properties for biomedical applications that cannot be obtained from in vivo studies.

References

1. Gubin, S.P.; Koksharov, Y.A.; Khomutov, G.; Yurkov, G.Y. Magnetic nanoparticles: Preparation, structure and properties. *Russ. Chem. Rev.* **2005**, *74*, 489–520. [CrossRef]
2. Taufiq, A.; Saputro, R.E.; Susanto, H.; Hidayat, N.; Sunaryono, S.; Amrillah, T.; Wijaya, H.W.; Mufti, N.; Simanjuntak, F.M. Synthesis of Fe_3O_4/Ag Nanohybrid Ferrofluids and Their Applications as Antimicrobial and Antifibrotic Agents. *Heliyon* **2020**, *6*, e05813. [CrossRef] [PubMed]
3. Sun, H.; Zeng, X.; Liu, M.; Elingarami, S.; Li, G.; Shen, B.; He, N. Synthesis of Size-Controlled Fe_3O_4@SiO_2 Magnetic Nanoparticles for Nucleic Acid Analysis. *J. Nanosci. Nanotechnol.* **2012**, *12*, 267–273. [CrossRef] [PubMed]
4. Shen, L.; Li, B.; Qiao, Y. Fe_3O_4 Nanoparticle in Targeted Drug/Gene Delivery Systems. *Materials* **2018**, *11*, 324. [CrossRef] [PubMed]
5. Prijic, S.; Sersa, G. Magnetic Nanoparticles as Targeted Delivery System in Oncology. *Radiol. Oncol.* **2011**, *45*, 1–16. [CrossRef] [PubMed]
6. Wulandari, I.O.; Sulistyarti, H.; Safitri, A.; Santjojo, D.J.D.H.; Sabarudin, A. Development of Synthesis Method of Magnetic Nanoparticles Modified by Oleic Acid and Chitosan as a Candidate for Drug Delivery Agent. *J. Appl. Pharm. Sci.* **2019**, *9*, 001–011.
7. Goya, G.F.; Morales, M.P. Field Dependence of Blocking Temperature in Magnetite Nanoparticles. *J. Metastable Nanocrystalline Mater.* **2004**, *20–21*, 673–678. [CrossRef]
8. Saragi, T.; Sinaga, H.D.; Rahmi, F.; Pramesti, G.A.; Sugiarto, A.; Therigan, A.; Syakir, N.; Hidayat, S.; Risdiana. Blocking Temperature of Magnetite Nanoparticles Fe_3O_4 Encapsulated Silicon Dioxide SiO_2. *Key Eng. Mater.* **2020**, *855*, 172–176. [CrossRef]
9. Hira, U.; Sher, F. Structural, Magnetic and High-Temperature Thermoelectric Properties of $La_{0.4}Bi_{0.4}Ca_{0.2}Mn_{1-x}Co_xO_3$ ($0 \leq x \leq 0.3$) Perovskites. *J. Magn. Magn. Mater.* **2018**, *452*, 64–72. [CrossRef]
10. Weaver, J.B.; Kuehlert, E. Measurement of Magnetic Nanoparticle Relaxation Time. *Med. Phys.* **2012**, *39*, 2765–2770. [CrossRef]
11. Wang, J.; Wu, W.; Zhao, F.; Zhao, G. Curie Temperature Reduction in SiO_2-coated Ultrafine Fe_3O_4 Nanoparticles: Quantitative Agreement with a Finite-Size Scaling Law. *Appl. Phys. Lett.* **2011**, *98*, 083107. [CrossRef]
12. Volkov, I.; Gudoshnikov, S.; Usov, N.; Volkov, A.; Moskvina, M.; Maresov, A.; Snigirev, O.; Tanaka, S. SQUID-Measurements of Relaxation Time of Fe_3O_4 Superparamagnetic Nanoparticle Assembles. *J. Magn. Magn. Mater.* **2006**, *300*, 294–297. [CrossRef]
13. Spizzo, F.; Sgarbossa, P.; Sieni, E.; Semenzato, A.; Dughiero, F.; Forzan, M.; Bertani, R.; Bianco, L.D. Synthesis of Ferrofluids Made of Iron Oxide Nanoflowers: Interplay Between Carrier Fluid and Magnetic Properties. *Nanomaterials* **2017**, *7*, 373. [CrossRef] [PubMed]
14. Del Bianco, L.; Lesci, I.G.; Fracasso, G.; Barucca, G.; Spizzo, F.; Tamisari, M.; Scotti, R.; Ciocca, L. Synthesis of Nanogranular Fe_3O_4/Biomimetic Hydroxyapatite for Potential Applications in Nanomedicine: Structural and Magnetic Characterization. *Mater. Res. Express* **2015**, *2*, 065002. [CrossRef]
15. Del Bianco, L.; Fiorani, D.; Testa, A.M.; Bonetti, E.; Savini, L.; Signoretti, S. Magnetothermal Behavior of a Nanoscale Fe/Fe Oxide Granular System. *Phys. Rev. B* **2002**, *66*, 174418. [CrossRef]
16. Saragi, T.; Permana, B.; Therigan, A.; Hidayat, S.; Syakir, N.; Risdiana. Physical Properties of Encapsulated Iron Oxide. *Mater. Sci. Forum* **2019**, *966*, 277–281. [CrossRef]
17. Blundell, S. *Magnetism in Condensed Matter*; Oxford University Press: New York, NY, USA, 2001.
18. Tang, Z.X.; Sorensen, C.M.; Klabunde, K.J. Size-Dependent Curie Temperature in Nanoscale $MnFe_2O_4$ Particles. *Phys. Rev. Lett.* **1991**, *67*, 3112. [CrossRef] [PubMed]
19. Zatsiupa, A.A.; Bashkirov, L.A.; Troyanchuk, I.O.; Petrov, G.S.; Galyas, A.I.; Lobanovsky, L.S.; Truhanov, S.V. Magnetization, Magnetic Suceptibility, Effetive Magnetic Moment of Fe^{3+} ions in $Bi_{25}FeO_{39}$ Ferrite. *J. Solid State Chem.* **2014**, *212*, 147–150. [CrossRef]

20. Osaci, M.; Abrudean, C.; Berdie, A. Relaxation Times in Magnetic Nanoparticle System and Memory Effects. *Acta Phys. Pol. A* **2007**, *112*, 1203–1212. [CrossRef]

21. Balaev, D.A.; Semenov, S.V.; Dubrovskivy, A.A.; Yakushkin, S.S.; Kirillov, V.L.; Martyanov, O.N. Superparamagnetic Blocking of an Ensemble of Magnetite Nanoparticles upon Interparticle Interactions. *J. Magn. Magn. Mater.* **2017**, *440*, 199–202. [CrossRef]

22. Krishnan, K.M. Biomedical Nanomagnetics: A Spin through Possibilities in Imaging, Diagnostics, and Therapy. *IEEE Trans. Magn.* **2010**, *46*, 2523–2558. [CrossRef] [PubMed]